Neurochemical Research (2019) 44:714–725
https://doi.org/10.1007/s11064-018-2694-5

ORIGINAL PAPER

Scalable Measurements of Intrinsic Excitability in Human iPS Cell-Derived Excitatory Neurons Using All-Optical Electrophysiology

Luis A. Williams[1] · Vaibhav Joshi[1] · Michael Murphy[1] · John Ferrante[1] · Christopher A. Werley[1] · Theodore Brookings[1] · Owen McManus[1] · Johannes Grosse[2] · Ceri H. Davies[3] · Graham T. Dempsey[1]

Received: 2 May 2018 / Revised: 2 December 2018 / Accepted: 4 December 2018 / Published online: 2 January 2019
© Springer Science+Business Media, LLC, part of Springer Nature 2019

Abstract

Induced pluripotent stem (iPS) cells offer the exciting opportunity for modeling neurological disorders in vitro in the context of a human genetic background. While significant progress has been made in advancing the use of iPS cell-based disease models, there remains an unmet need to characterize the electrophysiological profile of individual neurons with sufficient throughput to enable statistically robust assessment of disease phenotypes and pharmacological modulation. Here, we describe the Optopatch platform technology that utilizes optogenetics to both stimulate and record action potentials (APs) from human iPS cell-derived excitatory neurons with similar information content to manual patch clamp electrophysiology, but with ~ 3 orders of magnitude greater throughput. Cortical excitatory neurons were produced using the NGN2 transcriptional programming approach and cultured in the presence of rodent glial cells. Characterization of the neuronal preparations using immunocytochemistry and qRT-PCR assays reveals an enrichment of neuronal and glutamatergic markers as well as select ion channels. We demonstrate the scale of our intrinsic cellular excitability assay using pharmacological assessment with select ion channel modulators quinidine and retigabine, by measuring changes in both spike timing and waveform properties. The Optopatch platform in human iPS cell-derived cortical excitatory neurons has the potential for detailed phenotype and pharmacology evaluation, which can serve as the basis of cellular disease model exploration for drug discovery and phenotypic screening efforts.

Keywords Optogenetics · Electrophysiology · Induced pluripotent stem cells

Introduction

The impressive progress of neuroscience research over recent decades has not yet translated to improved treatments for patients with neurological diseases. The discrepancy between the massive private and academic investments in drug discovery for neurological and psychiatric diseases and the small and still declining number of novel drug approvals is a clear indicator of challenges faced by the field [1–3]. These challenges exist at all phases of drug discovery, from target validation and hypothesis generation via pre-clinical and genetic models through the design of clinical trials, use of biomarkers, and implementation of regulatory processes. The scale of the problem has resulted in adaptation of funding and regulatory policies as well as a reappraisal of disease concepts and their application to pre-clinical and clinical drug discovery [4–6].

The slow progress in neuroscience drug discovery has been attributed to several key challenges. First, there remains a lack of robust human model systems that translate to primary therapeutic endpoints. While there are many neurophysiological pathways that are well conserved in species used in pre-clinical tests [7, 8], these models have been historically poor predictors of efficacy in humans [9]. The use of animal models in drug discovery have led to a number

Special issue: In honor of Graham Collingridge.

✉ Ceri H. Davies
ceri.davies@takeda.com

✉ Graham T. Dempsey
graham.dempsey@qstatebio.com

[1] Q-State Biosciences, 179 Sidney Street, Cambridge, MA 02139, USA

[2] Takeda California, San Diego, USA

[3] Takeda Pharmaceuticals Company Limited, Shonan Health Innovation Park, 26-1 Muraoka Higashi 2-chome, Fujisawa, Kanagawa 251-8555, Japan

of clinical disappointments, in part due to a lack of strong validation of the animal model, which can lead to misinformation regarding efficacy of candidate therapies [10].

A second challenge in neuroscience drug discovery is creating causal connection between human genetics and clinical phenotypes. Some neurological disorders, such as epilepsy, now have clear links between specific genes and rare disease indications [11]. Other disorders are less clear. For example, in psychiatry, disease entities have been deconstructed to identify underlying neurophysiological abnormalities to stratify patients [12]. Human genetic data have been proposed for patient stratification as well as for demonstrating the relevance of molecular targets [13, 14]. Supported by the National Institute of Health's Research Domain Criteria initiative, researchers have identified a large overlap of genetic risk factors between psychiatric diseases including schizophrenia, major depression and bipolar disorders, which points towards common underlying mechanisms such as histone methylation, innate immunity and synaptic signaling [15, 16]. However, it is very difficult to associate particular mutations with well-defined clinical phenotypes. Similarly, for autism spectrum disorders where there is large phenotypic heterogeneity, the reductionist approach of robustly matching genetic risk factors with neuropsychiatric endophenotypes has not been straightforward. Patient stratification for phenotypically defined subgroups has not resulted in a reduced complexity of the genetic risk factors [17]. This issue highlights that clinical phenotypes are too complex to be predicted by individual genetic risk factors.

In a similar reductionist approach, current drug discovery programs are often geared towards modulation of a single drug target ignoring the fact that most clinically used CNS compounds act on several targets. Even where the indication can be clearly linked to a specific gene, as in epilepsy, it has been challenging to bring new therapies to market. Accepting the complexity of neurological diseases and their underlying risk factors, environmental as well as genetic, implies the necessity of introducing models bridging the gap between cellular processes on one hand and endophenotypes in animals or humans on the other.

Human induced pluripotent stem (iPS) cell-based models of disease have become a potentially powerful approach to modeling neurological disorders such as epilepsy [18], bipolar disorder [19] and ALS [20] in the context of a human genetic background. Human iPS cell-based technology makes it possible to compare the phenotype of differentiated neurons obtained from healthy individuals and disease patients and to correlate in vitro findings with clinical drug responses [21]. The characterization of patient iPS cell-derived neuronal cultures is bound to provide insights into the relationship between altered network features and diseases or behavioral domains [22, 23]. Furthermore, iPS cells are amenable to the use of CRISPR/Cas9 gene editing tools to make isogenic cellular models [24]. These models enable the phenotypic impact of gene mutations to be tested in a controlled genetic background, removing potential sources of variability between individual patient cell lines [25]. As such, stem cell technology is poised to make a major impact in neuroscience drug discovery [26].

To fully leverage human iPS cell-based neuronal models for drug screening requires measurement tools capable of assaying neuronal activity at scale. Such tools can be used for building phenotypic assays, which have long played an important role in drug discovery when a clear druggable target does not yet exist [27–29]. Many of the mechanisms underlying intrinsic spiking of individual neurons and synaptic communication between cells, the two primary modes of activity of the brain, have been studied by manual patch clamp whose throughput is too low for drug screening, but whose exquisite information content is powerful for exploring single-cell electrophysiology. Multi-electrode arrays (MEAs) offer higher throughput for measuring emergent network properties of neuronal cultures, but lack single-cell precision. Thus, there remains a need for high-throughput assays of single-cell electrophysiology, which is met by the Optopatch platform described here. Characterizing neuronal networks by massive parallel recording of neuronal activity has the potential to assess the utility of pharmacologically active compounds to modulate neurophysiological network behavior and to rescue disease phenotypes [30].

The abovementioned issues underscore the need for novel human cellular models and tools to rapidly study the relevant, complex electrical and synaptic behavior and neuronal phenotypes. In the studies presented here we explore the potential of an all-optical electrophysiological platform to capture the diversity of individual cellular activity patterns and responses to pharmacological interventions in human iPS cell-derived cortical excitatory neurons. Using optogenetics to both stimulate and record action potentials enabled the rapid recording of the electrical activity of 1000s of individual neurons and their pharmacological responses. By profiling established compounds and comparing their profiles to novel drug candidates, the complexity of neurological diseases with complex genetics can potentially be broken down without relying entirely on a reductionist model of a one-to-one relationship between genes and endophenotypes [31]. Furthermore, by providing improved scalable in vitro models of nervous system function and human pharmacology, novel iPS cell-based Optopatch assays can potentially pave the way to increased success in therapeutic discovery.

Materials and Methods

Human iPS Cell Culture and Production of iPS Cell-Derived NGN2 Excitatory Neurons

Control iPS cell lines "11a" and "20b" [32] were maintained in culture using mTeSR1™ medium (STEMCELL Technologies™) and Matrigel™ (Corning) coating according to manufacturers' protocols. iPS cell lines were differentiated into NGN2 excitatory neurons using a transcriptional programming approach [33], whereby iPS cell lines were initially modified via lentiviral delivery of a construct expressing the reverse tetracycline transactivator (rtTA) and a tetracycline-responsive (*TetOp*) construct driving the expression of the pro-neuronal transcription factor NGN2 and a puromycin resistant enzyme. Genetically modified iPS cell lines were expanded in mTeSR1™ medium for 3–5 passages prior to induction of NGN2. For neuronal production, iPS cells were dissociated with Accutase™ according to manufacturer's recommendations and plated at a density of 300,000 cells/cm^2 using mTeSR1™ medium supplemented with 10 µM Rock Inhibitor (Sigma) and 2 µg/mL doxycycline (Sigma) to initiate NGN2 overexpression. Differentiating cells were subsequently maintained for 3 days in 1:1 DMEM/F-12:Neurobasal Medium (ThermoFisher Scientific) supplemented with 1 × GlutaMAX, 1 × non-essential amino acids, 1 × N2 (Gibco), 1 × B-27, 2 µg/mL doxycycline (Sigma) and 2 µg/mL puromycin. This process resulted in a pure population of neurons that were dissociated with Accutase™ and plated at 80,000 cells/cm^2 onto poly-D-lysine/laminin pre-coated single-well (MatTek™) or 8-well (Ibidi) dishes for prolonged culture. Neuronal cultures were maintained until DIV18 in Neurobasal A Medium supplemented with 1 × GlutaMAX, 1 × non-essential amino acids, 1 × N2 (Gibco), 1 × B-27, 10 ng/mL BDNF (R&D) and 10 ng/mL GDNF (R&D). Three days after plating, neuronal cultures were supplemented with 40,000 cells/cm^2 of primary mouse glial cells, prepared as previously described [34]. One week prior to Optopatch measurements, neuronal cultures were switched to BrainPhys™ Neuronal medium (STEMCELL Technologies) supplemented with 1 × N2-A, 1 × SM1 (STEMCELL Technologies), 10 ng/mL BDNF (R&D) and 10 ng/mL GDNF (R&D).

Transduction of NGN2 Neurons with Optopatch Components

Lentiviral particles encoding Optopatch components CheRiff and QuasAr were produced in 293T cells as previously described [35]. Neuronal cultures were transduced on DIV10 with CheRiff-mOrange2 and QuasAr3-Citrine constructs driven by the *CAMK2A* promoter to target expression of the Optopatch components to mature excitatory neurons. QuasAr3-Citrine is a variant of QuasAr2 [36] which incorporates multiple $K_{ir}2.1$ trafficking sequences and a lysine (putative ubiquitination site) to arginine substitution at position 171, resulting in improved expression and trafficking [37]. Transduction of neuronal cultures was carried out as described before [35], with washing of the virus by 2 × medium exchanges 16–24 h after treatment (DIV11). Neuronal cultures were maintained until DIV25, when neurons were recorded using Optopatch imaging.

Immunocytochemistry and Quantitative Reverse Transcriptase Polymerase Chain Reaction (qRT-PCR) Characterization of NGN2 Neurons

For immunocytochemistry (ICC), neuronal cultures were fixed using cold 4% paraformaldehyde for 20 min and permeabilized with 0.2% Triton X-100. Dishes were blocked with 10% donkey serum in 0.1% PBS-Tween, incubated with primary antibodies overnight at 4 °C. After five washes with 0.1% PBS-Tween, dishes were treated with secondary (Alexa®-conjugated) antibodies for 1 h at room temperature. Cell nuclei (DNA) were stained with Hoechst® 33342. Primary antibodies used in this study were human nuclear-specific antibody (Millipore; MAB1281, 1:1000), mature pan-neuronal marker MAP2 (Abcam; ab5392, 1:3000) and GABA (Sigma; A2052, 1:1000). For ICC quantification of relevant markers, we used an epifluorescence microscope (ZEISS Axio Observer.A1) to acquire images with a 20 × objective lens from at least 4 fields of view per neuronal culture sample and two independent rounds of neuronal production. Images were contrasted and pseudo-colored using Adobe Photoshop. No statistical comparisons were conducted between the results obtained for the two different genotypes of neurons assayed.

For qRT-PCR, neuronal cultures were treated with TriZol Reagent (ThermoFisher Scientific) on DIV25. Total RNA was obtained from TriZol-preserved samples using manufacturer's protocol. RNA concentration and quality were determined using a NanoDrop. cDNA samples were prepared using 100 ng of RNA per sample and the iScript cDNA Synthesis Kit (BioRad®). cDNA was diluted 1:5 and gene targets were amplified using IDT® pre-designed human-specific primers and the iTaq SYBR® Green system (BioRad®) on the CFX96 Touch™ platform. Quantitation cycle (*Cq*) values, (a cycle in which fluorescence can be detected above background) were calculated for each target gene. Values obtained for iPS cell lines were used as reference.

Optopatch Imaging and Analysis

Prior to Optopatch imaging, cultured neurons in either single-well or 8-well format were aspirated to remove culture media. Cells were then rinsed with 1 mL of imaging buffer consisting of: 125 mM NaCl, 3 mM KCl, 3 mM $CaCl_2$, 1 mM $MgCl_2$, 10 mM HEPES, 30 mM glucose and synaptic blockers (10 µM NBQX, 25 µM D-AP5, 20 µM Gabazine to block AMPA, NMDA and GABA currents, respectively). Cells were aspirated again before addition of 1 mL of the imaging buffer and kept at room temperature for 15 min prior to imaging. The imaging buffer was chosen to reduce background autofluorescence and to maintain stable physiological conditions at ambient CO_2. The presence of synaptic blockers enables measurement of cell-autonomous spontaneous and evoked neuronal activity.

For pharmacological characterization, compound solutions were prepared fresh daily from DMSO stock solutions. Cells were aspirated and then incubated in imaging buffer in the presence of compound at the indicated concentration for 15 min prior to imaging. The final DMSO concentration was limited to 0.2% V/V at the highest compound concentrations tested.

Optopatch imaging was performed on a custom built, ultra-widefield fluorescence microscope described previously [35, 38]. Briefly, samples were illuminated with 1) ~ 100 W/cm^2 635 nm laser excitation (Dilas) to monitor changes in membrane potential through changes in QuasAr fluorescence and 2) variable blue light intensity (0–110 mW/cm^2, 470 nm LED, Luminus) to depolarize the neuronal membrane through CheRiff. Custom blue light stimulus protocols were used to probe different facets of the electrophysiological response, as described in the text. Imaging data were recorded on a Hamamatsu ORCA-Flash 4.0 sCMOS camera across a 4 mm × 0.5 mm field of view at a 1 kHz frame rate. Data acquisition was performed using custom control software written in MATLAB.

The Optopatch data analysis pipeline, written primarily in MATLAB, has been described elsewhere [35]. Briefly, Optopatch movies were first segmented using temporal principle component analysis (PCA) followed by spatial–temporal independent component analysis (ICA) to identify individual neurons. Fluorescence-time traces were extracted for each putative neuron, and selection criteria were used to reject sources where the signal-to-noise ratio was too low (e.g. SNR < 3) or where the cell size was too small (e.g. diameter < 10 µm). A custom spike-finding algorithm then identified action potentials and calculated their shape and timing properties, as described previously [35]. For action potential shape properties, the width, rise time and after-hyperpolarization were computed as follows: action potential width was measured at 80% below the action potential peak towards the onset (spike onset is defined as the point of maximum 2nd derivative before the spike peak); spike rise time is measured as the time between spike onset and spike peak; and spike after-hyperpolarization was assessed as the maximal extent of the trace below onset after a spike, expressed as a fraction of spike height. Spike frequency is computed simply as the number of spikes detected during the stimulation pulse of fixed duration (500 ms) [35]. Statistical significance/p-values were determined using the Kolmogorov–Smirnov statistic with a custom MATLAB routine [35]. Briefly, the degree of difference between two groups, in this case two populations of neurons treated with two different concentrations of pharmacological compound, is measured using the Kolmogorov–Smirnov (KS) statistic. p-values are calculated using a permutation test, where a null distribution is built by iteratively computing KS statistics for data with scrambled labels and comparing the KS statistic for the real data to this null distribution. At least 1000 permutations are measured for the permutation test, and corrections are made for multiple comparisons before reporting [35]. In the figures, "*", "**" or "***" denote p values of $p < 0.05$, $p < 0.01$ and $p < 0.001$, respectively; with all reported error bars indicating standard error of the mean.

Results

To characterize the intrinsic excitability activity of human iPS cell-derived excitatory neurons with the Optopatch platform (Fig. 1), we used two iPS cell lines, "11a" and "20b". These two iPS cell lines were derived from two neurologically healthy male subjects [32]. Characterization of these two cell lines, including their differentiation into CNS neurons has been described previously [32]. 11a and 20b iPS cells were converted into excitatory neurons using a transcriptional programming approach whereby the pro-neuronal transcription factor NEUROGENIN2 (NGN2) is overexpressed using doxycycline responsive lentiviral constructs (Fig. 1). This process drives the rapid conversion of iPS cells into neurons that resemble cortical excitatory neurons [33]. Co-culture with primary rodent glia facilitates neuronal electrophysiological maturation. To enable Optopatch measurements, we transduced the neuronal cultures (DIV10) with lentiviral constructs expressing Optopatch components driven by the neuronal excitatory promoter *CAMK2A* and recorded from the cells 2 weeks later (Fig. 1). At the time of Optopatch measurements, the NGN2 excitatory neuron and glial co-cultures were morphologically homogeneous and electrophysiologically active, yielding highly stereotyped and reproducible data across cells, dishes, differentiation rounds and cell lines.

To confirm effective conversion of iPS cells from both genetic backgrounds into excitatory neurons, we used immunocytochemistry (ICC) to characterize the iPS cell-derived

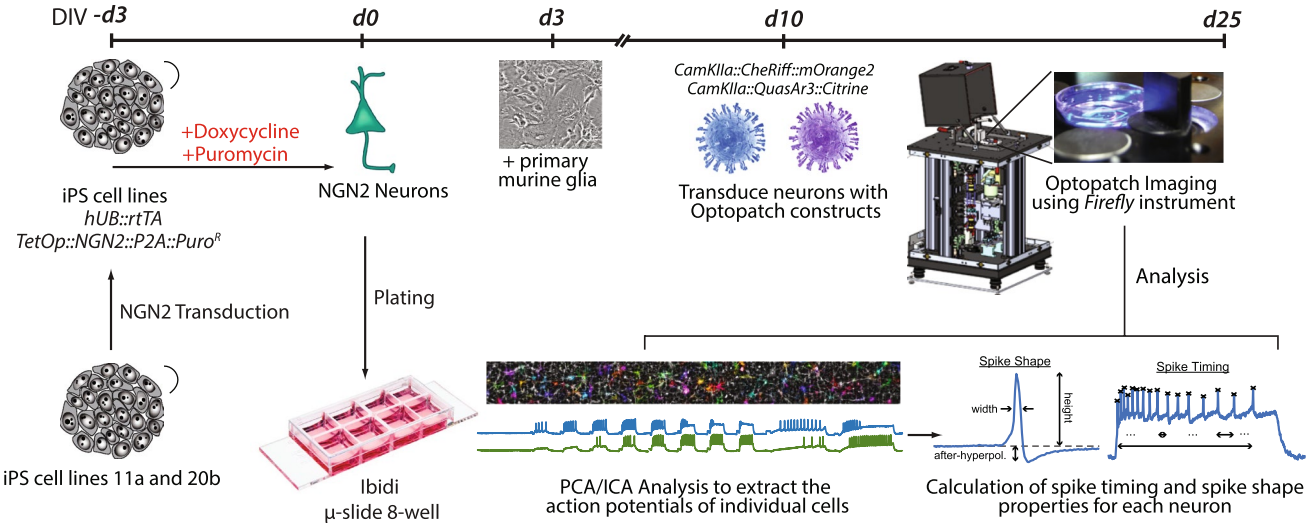


Fig. 1 Optopatch platform workflow in human induced pluripotent stem (iPS) cell-derived NGN2 excitatory neurons. NGN2 neurons are produced using a transcriptional programming approach. iPS cell lines are initially modified by transduction of a construct expressing the reverse tetracycline transactivator (rtTA) driven by the *UBIQUITIN* (*hUB*) promoter and a tetracycline-responsive (*TetOp*) construct driving the expression of the pro-neuronal transcription factor NGN2 and a Puromycin resistant enzyme. NGN2 expression (via doxycycline) and puromycin selection for 3 days result in a pure population of NGN2 neurons, which are then plated onto single well or 8-well dishes for prolonged culture. NGN2 neurons are co-cultured with primary murine glia to promote neuronal maturation. Neurons are later transduced with lentiviral constructs encoding the Optopatch components CheRiff-mOrange2 and QuasAr3-Citrine. After 25 days or more in culture, NGN2 electrophysiology can be measured using the Optopatch Firefly instrument. Downstream analyses of the Optopatch data include image segmentation to define neural sources, automated spike finding and extraction of spike shape and timing properties. (Color figure online)

neuronal preparations at the time of electrophysiological measurements (DIV25). To determine neuronal production efficiency, cultures were immunostained using antibodies against a human-specific nuclear antigen (hNuclei) and the mature pan-neuronal cytoskeletal protein microtubule-associated protein 2 (MAP2) (Fig. 2a). We then estimated the percentage of human differentiated cells in the cultures corresponding to neurons by calculating percentage of MAP2 + cells over hNuclei + cells. Large nuclei not stained with the hNuclei immunoreagent (Fig. 2a) correspond to nuclei of murine glial cells used as a supportive monolayer. We found that > 94% of human differentiated cells expressed the MAP2 protein, which showed the expected localization in proximal neurites (Fig. 2a, b), indicating successful neuronal production. We also used an antibody against the inhibitory neurotransmitter GABA to determine the fraction of GABAergic neurons in the cultures at the time of Optopatch measurements. Consistent with previous studies reporting enrichment for excitatory neurons when using an NGN2-mediated programming approach [33, 39], we found that only < 4% of human differentiated neurons (MAP2 + cells) in the NGN2 neuronal/mouse glia co-cultures showed strong immunoreactivity to the GABA antibody (Fig. 2c, d).

To further characterize the neuronal preparations at the time of Optopatch measurements, we obtained total RNA and subsequently synthesized cDNA from the human differentiated neuronal and mouse glia co-cultures. We then carried out qPCR assays to determine relative transcript abundance for a subset of pan-neuronal and neuronal type specific genes using primers selectively targeting the human transcripts. We calculated the quantitation Cycle (*Cq*) values for these genes, whereby low *Cq* values indicate initial enrichment of the specific target transcript molecules. Figure 2e shows a heat map of mean *Cq* values for eight cell-type specific genes and two housekeeping genes (*ACTB* and *GAPDH*). qRT-PCR assays showed that most cell-type specific genes are detected in the predicted pattern of enrichment. We observed significant enrichment of the pluripotency gene *NANOG* in iPS cells and of the pan-neuronal and excitatory genes *MAP2, SYN1, CAMK2A, SLC17A7* (vGLUT1) in the NGN2 neuronal culture samples. As a control sample for a different human iPS cell-derived neuronal type, we generated cDNA from 20b human differentiated neurons produced using a small molecule-based directed differentiation approach enriching for cortical GABAergic neurons [40]. Consistent with their predicted neuronal identity, *Cq* values for this inhibitory 20b sample suggest enrichment for gene transcripts encoding components of the GABA synthesis (*GAD1* and *GAD2*) and vesicle transport (*SLC32A1*/vGAT) pathways (Fig. 2e). To help inform pharmacological assessment of the neurons, we also carried out

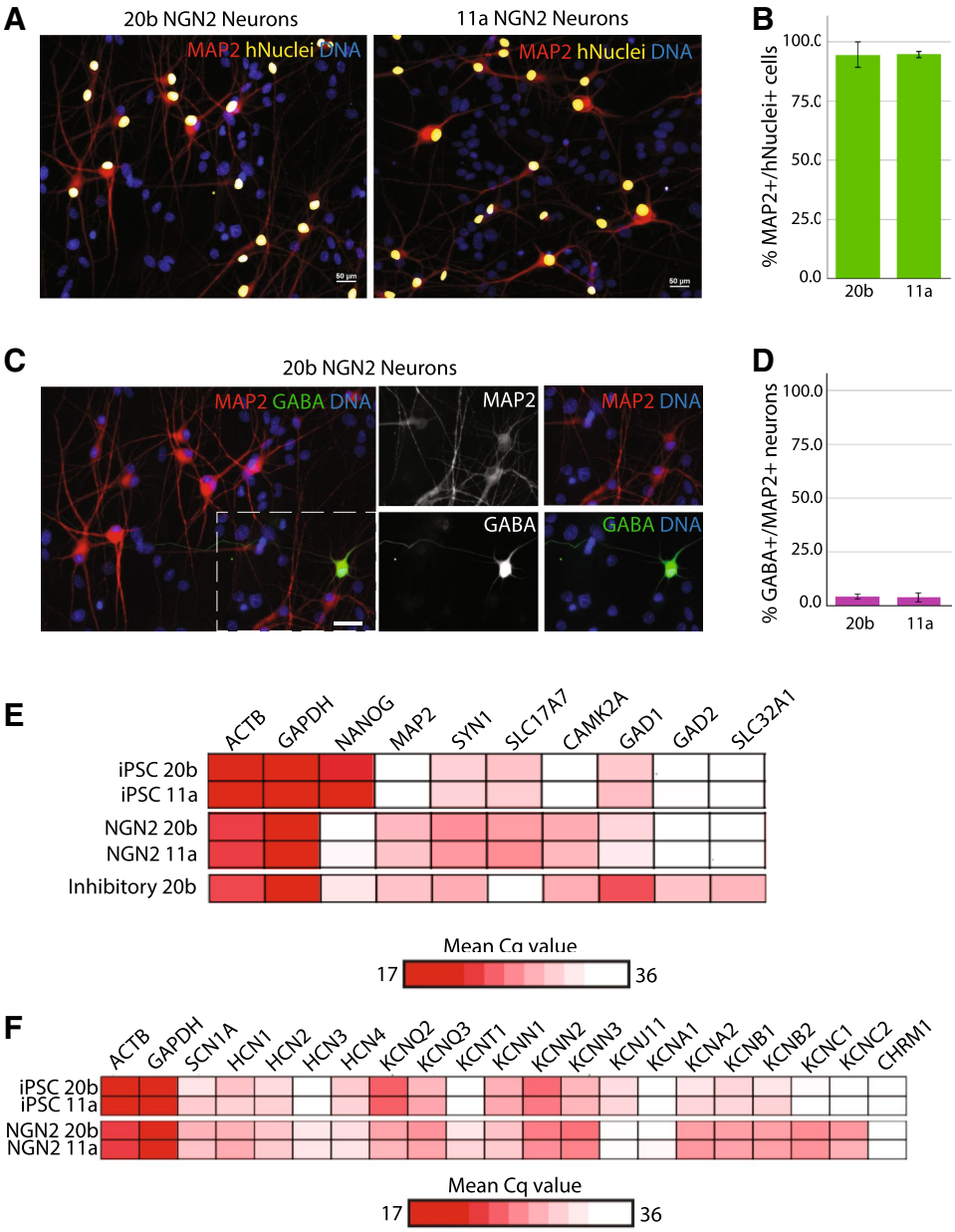


Fig. 2 Characterization of iPS cell-derived NGN2 neurons using immunocytochemistry (ICC) and qRT-PCR. **a** Fluorescence images of NGN2 neurons from two control genetic background iPS cell lines '20b' and '11a' immunostained for MAP2 (red), human nuclei (yellow) and DNA (blue). **b** Quantification of the ICC images shows that > 94% of human differentiated cells (hNuclei+) in the cultures express the pan-neuronal marker MAP2, indicating successful production of neurons. **c** Fluorescence images of NGN2 neurons from control background 20b stained for GABA (green) in addition to MAP2 (red) and DNA (blue). Panels of the different markers are shown for the region highlighted by the dotted line. **d** Quantification of the ICC images indicates that only < 4% of cells identified as neurons showed immunoreactivity against the GABA antibody, consistent with the expected enrichment for excitatory neurons. **e** Heat map quantification of Cq values for select genes in iPS cell lines and differentiated neurons showing enrichment for selected pan-neuronal and excitatory transcripts in the neuronal cultures. **f** Heat map quantification of Cq values for select ion channel targets in both the starting iPS cell lines (11a and 20b) and the derived NGN2 neurons for each genetic background. Neurons were cultured to DIV25 in the presence of rodent astrocytes prior to characterization with qPCR. (Color figure online)

qPCR-based assessment of relative transcript abundance for a subset of genes encoding potential pharmacological targets. These targets included sodium and potassium channels, and hyperpolarization-activated and cyclic nucleotide-gated (HCN) channels. A heat map of average Cq values suggests that, except for *KCNJ11, KCNA1*, and *CHRM1* with Cq > 34, most of the genes encoding the selected pharmacological targets were detected at low levels (Cq > 28) (Fig. 2f).

All optical measurements of electrophysiology, *Optopatch* [35, 36], rely on the expression of the voltage actuator CheRiff, which elicits action potentials upon blue-light stimulation, and the voltage reporter QuasAr, which generates near infrared fluorescence emission as result of changes in membrane potential (Fig. 3a). Each of these two components is fused to a fluorescent protein used to monitor reporter expression levels and membrane trafficking [35, 36] (Fig. 3a, b). We routinely observed robust and neuronal-specific expression of fluorescent reporters mOrange2, fused to CheRiff, and Citrine, fused to QuasAr in the neuronal preparations at the time of Optopatch characterization (Fig. 3b).

As described previously [35], Optopatch measurements were carried out in a custom-built ultra-widefield fluorescence microscope, the *Firefly* [38] (Fig. 1). Using this platform, we recorded the intrinsic excitability properties of 11a and 20b NGN2 neuronal cultures at DIV25 in the presence of synaptic blockers NBQX, D-AP5 and Gabazine to block AMPA, NMDA and GABA currents, respectively. A custom blue light stimulus protocol of three 500 ms blue light steps of increasing intensity (1, 15 and 75 mW/cm^2) followed by two 2 s ramps of linearly increasing intensity (0.5–10 mW/cm^2 and 0.5–110 mW/cm^2) was used to elicit a range of activity from individual neurons (Fig. 3c). ~50 to 100 neurons were simultaneously stimulated and recorded in a single field of view (see methods for analysis details). High signal-to-noise ratio (SNR) fluorescence-time traces were generated (Fig. 3c), and action potentials could be detected with high fidelity. Individual action potentials detected for each of the hundreds of neurons recorded with Optopatch are shown in a spike raster plot (Fig. 3d), where each row represents a single neuron, and each dot represents a detected spike. While individual neurons showed a diversity of spiking behavior throughout the stimulus protocol, the average firing rate of the population (435 neurons for 11a and 393 neurons for 20b) was remarkably similar for both cell lines (Fig. 3e). These data demonstrated the overall consistency of neuronal production between the two cell lines in generating electrophysiologically active cells with remarkably similar performance in our Optopatch assay.

We next tested the sensitivity of our excitability assay for detecting pharmacological modulation in NGN2 neurons using the well-characterized compound quinidine, which is reported to increase spike width and reduce spike activity [41]. Consistent with the anticipated effect, acute addition of quinidine to the NGN2 neurons resulted in dramatic changes to both the spike waveform and firing rate. These changes can be observed in the individual traces at 10 µM and 30 µM quinidine (Fig. 4a). By comparing the mean firing rate for neuronal cultures treated with different concentrations of quinidine with that of cultures treated with vehicle we detected a dramatic reduction in spike rate with increased blue light stimulus (Fig. 4b, c).

Lastly, we performed additional quantification of both the response to quinidine and retigabine in our Optopatch excitability assay. Quinidine has been reported to block several voltage-, Na^+ and Ca^{++} gated potassium channels ($K_{Na}1.1$, $K_{Ca}5.1$, $K_{2P}16.1$, $K_v1.5$, $K_v1.7$, $K_v10.1$, $K_v10.2$) [42] including two-pore forming channels as well as voltage gated Na^+ channels. The *KCNT1* gene encoding $K_{Na}1.1$ showed detectable expression levels in the NGN2 neurons compared to the starting iPS cell lines (Fig. 2f). The complex pharmacological activity of quinidine caused a concentration dependent broadening of the spikes (Fig. 5a). The spike width (measured from the base of the action potential) increased from 8.0 ± 0.2 to 17.7 ± 0.6 ms ($p < 0.001$), the spike rise time (measured from start to peak of the action potential) increased from 4.6 ± 0.8 to 7.2 ± 0.2 ms ($p < 0.001$), the time to the maximum of the after hyperpolarization (AhP) depth increased from 16.6 ± 0.3 to 26.0 ± 0.6 ms ($p < 0.001$) and the magnitude of the AhP depth (measured from the baseline fluorescence before the action potential) decreased from 0.20 ± 0.01 to 0.12 ± 0.02 (normalized fluorescence; $p < 0.001$), all at the maximum concentration tested (30 µM). At higher stimulation intensities (15 and 75 mW/cm^2), a concentration dependent reduction in the spike rate was also observed (Fig. 5a). At the highest concentration of quinidine (30 µM) and the peak intensity (75 mW/cm^2), the spike frequency reduced from 16.9 ± 0.6 to 6.6 ± 0.5 Hz ($p < 0.001$).

Retigabine is an activator of $K_v7.2/3/4/5$ potassium channels with efficacious concentrations in the low micromolar and nanomolar range (e.g. $K_v7.3$ EC_{50} 6.31×10^{-7} M; $K_v7.2$ 2.5×10^{-6} M) [42]. Treatment of NGN2 neurons with retigabine results in a deepening of the afterhyperpolarization (Fig. 5b) via enhanced M-currents which act as a brake on repetitive spiking and burst generation [43]. In line with this modulatory role of the M-currents we observed a concentration dependent reduction of the spike frequency at 15 and 75 mW/cm^2 stimulation intensities (Fig. 5b). At the highest concentration of retigabine (30 µM) and the peak intensity (75 mW/cm^2), the spike frequency reduced from 16.9 ± 0.6 to 8.2 ± 0.8 Hz ($p < 0.001$). We did observe subtle, but measurable changes in several action potential shape parameters at the highest concentration: spike width decreased from 8.0 ± 0.2 to 7.6 ± 0.2 ms, spike rise time decreased from 4.6 ± 0.8 to 4.1 ± 0.1 ms, the time to the maximum of the after hyperpolarization (AhP) depth decreased from 16.6 ± 0.3 to 15.1 ± 0.7 ms and the magnitude of the AhP depth increased from 0.20 ± 0.01 to 0.26 ± 0.03 (normalized fluorescence). The detectable expression levels of *KCNQ2* and *KCNQ3* transcripts in NGN2 neurons (Fig. 2f) are consistent with the strong pharmacological effect of retigabine. In total, our qPCR and Optopatch excitability assay results were consistent with the detection of pharmacological modulation from both quinidine and retigabine through ion channel targets expressed in the NGN2 neurons.

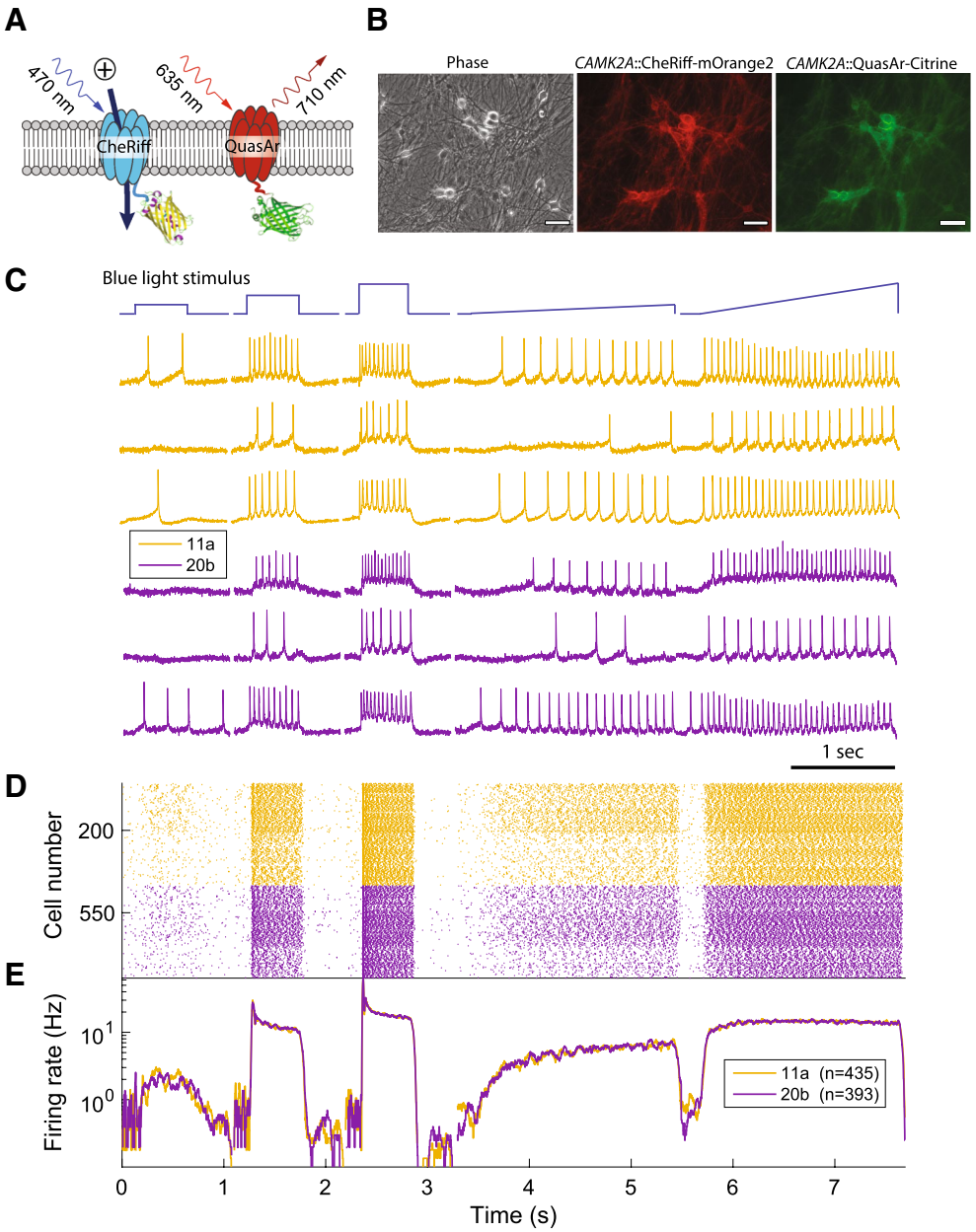


Fig. 3 Overview of Optopatch excitability assay in NGN2 neurons. **a** Cartoon representation of Optopatch proteins CheRiff and QuasAr. CheRiff is a blue-light gated ion channel. Illumination of neurons expressing CheRiff with 470 nm blue light leads to an influx of ions and subsequent depolarization of the cellular membrane. QuasAr is a red-light excitable voltage sensor. Illumination of neurons expressing QuasAr with 635 nm red light enables fluorescent detection of changes in membrane potential. When co-expressed, these proteins enable all-optical electrophysiology for simultaneous stimulation and detection of single-cell electrical activity. **b** Phase contrast images of NGN2 neurons in culture. Fluorescence images are shown for the same neurons expressing Optopatch constructs under the *CAMK2A* promoter. mOrange2 and Citrine were used to detect CheRiff (red) and QuasAr (green) expression, respectively. **c** Representative Optopatch fluorescence traces of single spiking neurons derived from control iPS cell lines 11a (yellow) and 20b (purple). The stimulus protocol used to elicit action potentials is shown above the traces: three, 500 msec duration steps of 1, 15 and 75 mW/cm^2, followed by two, 2 s duration ramps ranging from 0.5 to 10 mW/cm^2 followed by 0.5–110 mW/cm^2. **d** Spike raster plot showing the identified spikes for each neuron in the set of recordings for each. Each row of the plot corresponds to one cell and each dot corresponds to an identified action potential. **e** Average firing rate calculated across the stimulus protocol for each control cell line. 'n' indicates the number of single-cell neuronal recordings included in the statistics. (Color figure online)

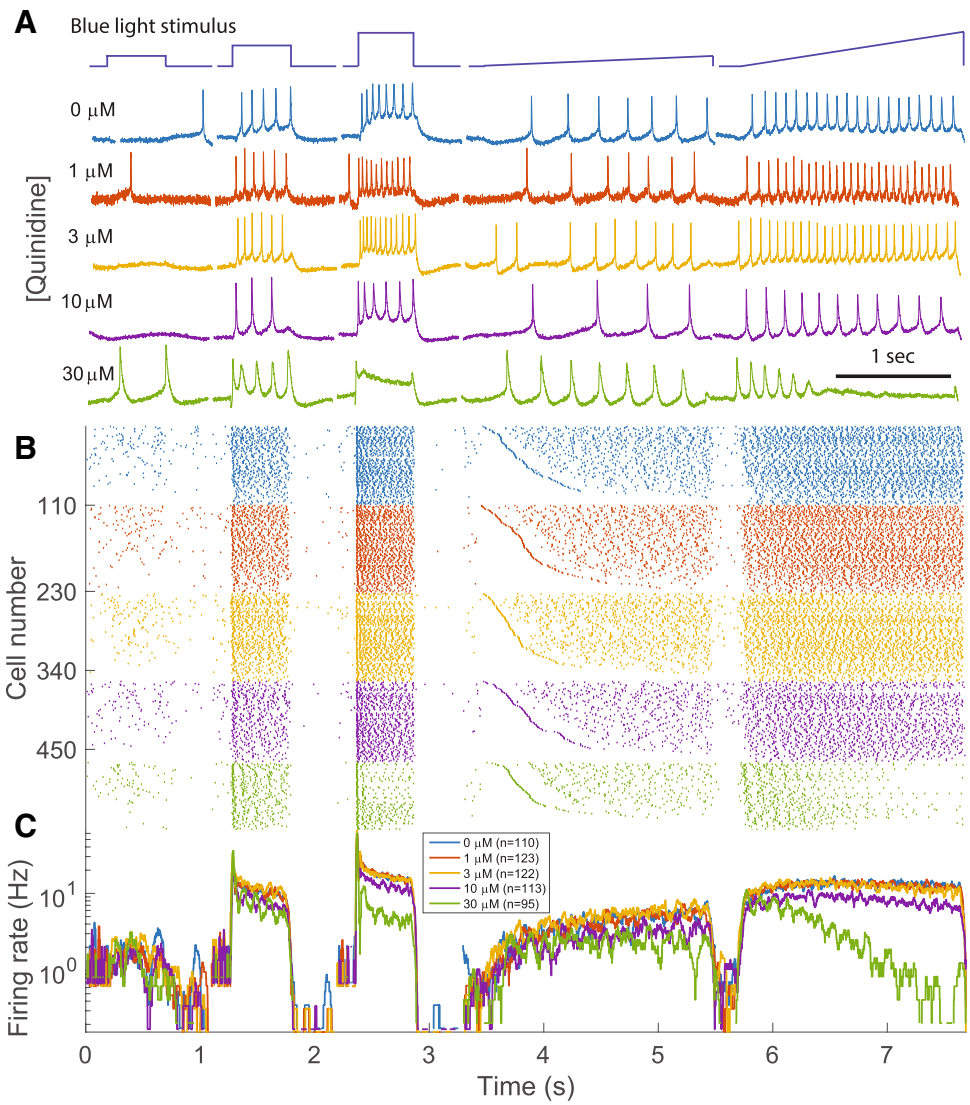


Fig. 4 Pharmacological response of NGN2 neurons to quinidine. **a** Representative Optopatch fluorescence traces of single spiking neurons derived from control iPS cell line 11a in response to escalating concentrations of the compound quinidine, from 0 μM (vehicle = 0.2% DMSO) to 30 μM. The stimulus protocol used to elicit action potentials is shown above the traces: three, 500 ms duration steps of 1, 15 and 75 mW/cm^2, followed by two, 2 s duration ramps ranging from 0.5 to 10 mW/cm^2 followed by 0.5–110 mW/cm^2. **b** Spike raster plot showing the identified spikes for each neuron in the set of recordings. Each row of the plot corresponds to one cell and each dot corresponds to an identified action potential. For each quinidine concentration, the cells are sorted by the timing of the first action potential in the first ramped stimulus. The gap following the first action potential highlights the initial spike rate. **c** Average firing rate calculated across the stimulus protocol for each concentration of quinidine. 'n' indicates the number of single-cell neuronal recordings included in the statistics. (Color figure online)

Discussion

Here, we have demonstrated a platform for production and electrophysiological characterization of NGN2 excitatory neurons derived from human induced pluripotent stem cells. The use of Optopatch technology enabled recordings of spike timing and shape properties from thousands of individual neurons with millisecond temporal resolution and single-cell spatial resolution. The electrophysiological responses of individual neurons showed a large degree of heterogeneity. However, by recording from hundreds of neurons with single-cell precision, we were able to explore the diversity of firing patterns in a statistically robust format. Furthermore, the demonstrated throughput of single-cell recordings for pharmacological evaluation of human iPS cell-derived neurons was ~ 2000 cells per hour, ~ 1000-fold higher than manual patch clamp recordings. This throughput of single-cell recordings is unmatched to date.

Interestingly, the two control cell lines, 11a and 20b, showed remarkably similar average spiking behavior despite all the potential confounding sources of biological and experimental variability such as genetic background, reprogramming and clonal selection, differentiation and neuronal plating [44]. A unique advantage of the NGN2 differentiation approach is the reduced time required for execution of neuronal production that enables a high degree of reproducibility between different human iPS cell lines. This process can be further industrialized by cryopreserving large batches of neurons for consistency during the execution of high-throughput assays. We believe these advantages will facilitate the use of these neuronal reagents as substrates for industrial drug screening campaigns with methods such as the Optopatch excitability assay presented here. Therefore, an understanding of the electrophysiological and pharmacological profile of these neurons is of high value toward these efforts.

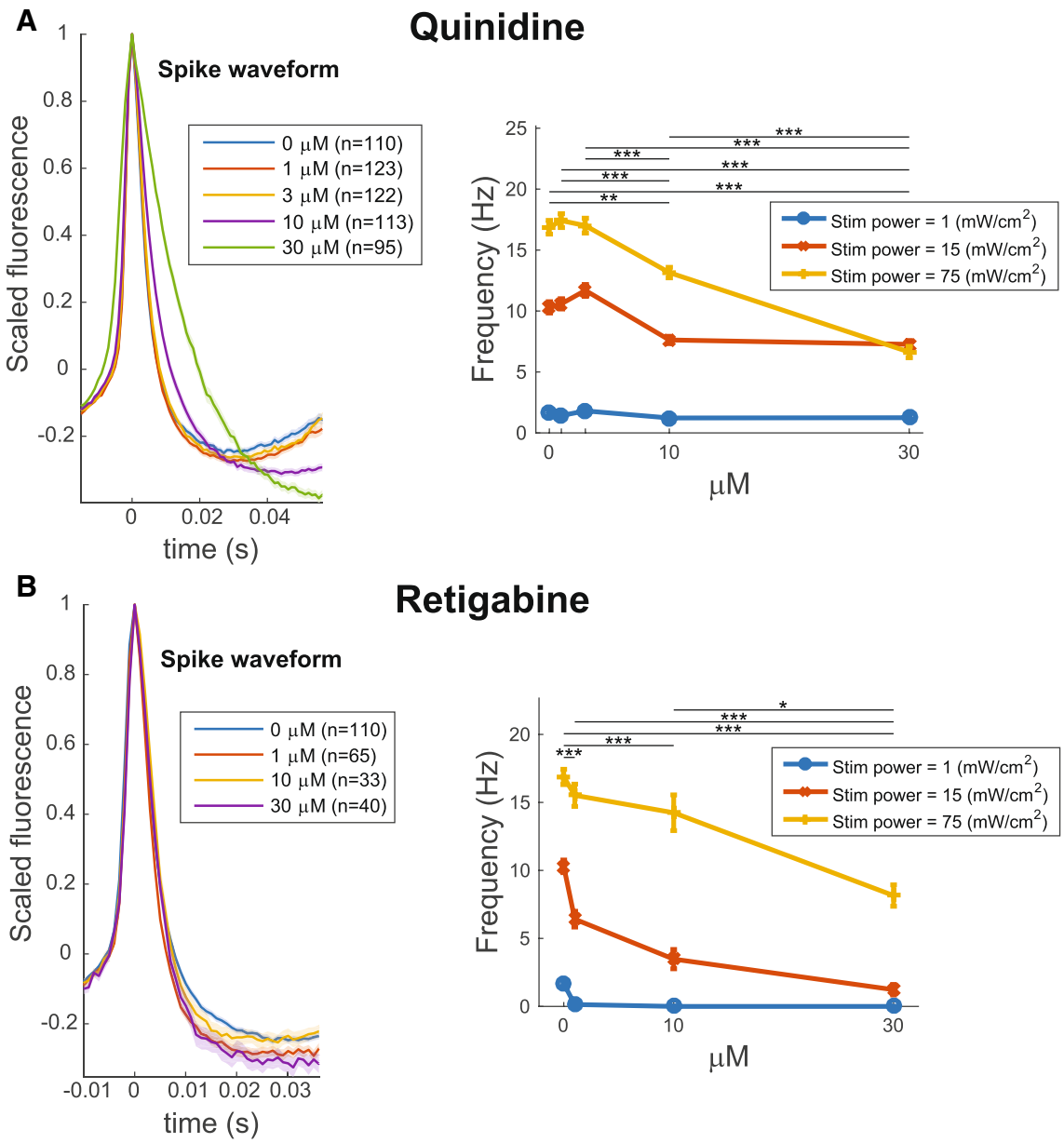


Fig. 5 Pharmacological characterization against select ion channel targets. Quantification of select electrophysiological properties of NGN2 neurons in response to **a** quinidine and **b** retigabine in the Optopatch excitability assay. **a** Quinidine shows pharmacological block of both Na^+ and K^+ channels. The spike waveform shows a strong concentration-dependent change in spike width and a reduction in spike frequency during the step portion of the protocol, particularly at higher stimulus intensities. **b** Retigabine is a Kv7.2/7.3 activator. Retigabine addition leads to a small, but detectable increase in the AhP depth and a dramatic reduction in spike rate at all concentrations tested. 0 μM condition = vehicle (0.2% DMSO). The blue light stimulus intensities are indicated in the right panels of **a** and **b**. (Color figure online)

Using two well-characterized pharmacological agents, quinidine and retigabine, we detected dramatic changes to electrophysiological parameters using our all-optical electrophysiology assay. The observed changes to both spike waveform and timing properties were consistent with the known activity of each compound against the respective channel targets. Expression of the genes encoding the pharmacological targets was confirmed in our preparations of NGN2 neurons. The ability to characterize pharmacological effects in human differentiated neurons is critical to developing new therapies. The clinical efficacy of quinidine, for example, is difficult to predict due to the complex pharmacology, and direct measurement of its impact on neuronal activity and action potential shape properties is an important step in elucidating relevant mechanisms. Although we only discussed a handful of intuitive electrophysiological characteristics,

the automated analysis extracts > 100 parameters describing spike shape and timing in different stimulus regimes. This rich, multidimensional data can be used to fingerprint different drug mechanisms for both promising molecular targets and known neurotoxic pathway (e.g. those that induce seizures). As new candidate therapeutics are characterized with Optopatch, the fraction of their overall effects mapping onto each of the known patterns may enable rapid prediction of drug mechanism and potential toxicity.

To complement the cell-autonomous excitability measurements described here, current efforts are underway to develop an Optopatch assay for synaptic transmission by expressing CheRiff in pre-synaptic neurons and QuasAr in post-synaptic neurons. Both assays are being developed in 96-well plates for high-throughput screening applications on a recently completed Firefly microscope which is compatible with microtiter plates. The development of large scale, high information content electrophysiological assays in human iPS cell-derived neurons using Optopatch will enable future phenotypic drug screens in patient-specific cellular models. Such tools have tremendous potential of advancing the overall goal of delivering new therapies to patients with diseases of the nervous system.

Acknowledgements L.A.W., V.J., J.F., C.A.W., O.M. and G.T.D. are employees of Q-State Biosciences. J.G. and C.H.D. are employees of Takeda Pharmaceuticals. We thank Dr. Steven Ryan (Q-State Biosciences) for assistance with revisions of the manuscript.

References

1. Gribkoff VK, Kaczmarek LK (2017) The need for new approaches in CNS drug discovery: why drugs have failed, and what can be done to improve outcomes. Neuropharmacology 120:11–19. https://doi.org/10.1016/j.neuropharm.2016.03.021
2. Forray C, Buller R (2017) Challenges and opportunities for the development of new antipsychotic drugs. Biochem Pharmacol 143:10–24. https://doi.org/10.1016/j.bcp.2017.05.009
3. Keshavan MS, Lawler AN, Nasrallah HA, Tandon R (2017) New drug developments in psychosis: challenges, opportunities and strategies. Prog Neurobiol 152:3–20. https://doi.org/10.1016/j.pneurobio.2016.07.004
4. Pankevich DE, Altevogt BM, Dunlop J et al (2014) Improving and accelerating drug development for nervous system disorders. Neuron 84:546–553. https://doi.org/10.1016/j.neuron.2014.10.007
5. Choi DW, Armitage R, Brady LS et al (2013) Medicines for the mind: policy-based "' Pull"' incentives for creating breakthrough CNS drugs. Neuron 84:554–563. https://doi.org/10.1016/j.neuron.2014.10.027
6. Butlen-ducuing F, Pétavy F, Guizzaro L et al (2016) Challenges in drug development for central nervous system disorders: a European Medicines Agency perspective. Nat Rev Drug Discov 15:813–814. https://doi.org/10.1038/nrd.2016.237
7. Millan MJ, Goodwin GM, Meyer-lindenberg A, Ove S (2015) Learning from the past and looking to the future: emerging perspectives for improving the treatment of psychiatric disorders. Eur Neuropsychopharmacol. https://doi.org/10.1016/j.euroneuro.2015.01.016
8. Kaiser T, Feng G (2015) Modeling psychiatric disorders for developing effective treatments. Nat Med 21:979–988. https://doi.org/10.1038/nm.3935
9. Forum on Neuroscience and Nervous System Disorders, Board on Health Sciences Policy, Institute of Medicine (2014) Improving and accelerating therapeutic development for nervous system disorders: workshop summary. National Academies Press, Washington, DC. Available from: https://www.ncbi.nlm.nih.gov/books/NBK169736/
10. Eisen JA, Ganley E, Maccallum CJ (2014) Open science and reporting animal studies: who' s accountable ? PLoS Biol 12:1–3. https://doi.org/10.1371/journal
11. Holmes GL, Noebels JL (2016) The epilepsy spectrum: targeting future research challenges. Cold Spring Harb Perspect Med. https://doi.org/10.1101/cshperspect.a028043
12. Insel T (2014) The NIMH research domain criteria (RDoC) project: precision medicine for psychiatry. Am J Psychiatry 171(4):395–397
13. Papassotiropoulos A, Quervain DJ, De (2015) Failed drug discovery in psychiatry: time for human genome-guided solutions. Trends Cogn Sci 19:183–187. https://doi.org/10.1016/j.tics.2015.02.002
14. Matsumoto M, Walton NM, Yamada H et al (2017) The impact of genetics on future drug discovery in schizophrenia. Expert Opin Drug Discov 12:673–686. https://doi.org/10.1080/17460441.2017.1324419
15. Breen G, Li Q, Roth BL et al (2016) Translating genome-wide association findings into new therapeutics for psychiatry. Nat Nuerosci 19(11):1392
16. PsychiatricGenomicsConsortium (2015) Psychiatric genome-wide association study analyses implicate neuronal, immune and histone pathways. Nat Neurosci. https://doi.org/10.1038/nn.3922
17. Chaste P, Klei L, Sanders SJ et al (2015) A genome-wide association study of autism using the Simons simplex collection: does reducing phenotypic heterogeneity in autism increase genetic homogeneity? Biol Psychiatry 77:775–784. https://doi.org/10.1016/j.biopsych.2014.09.017
18. Liu Y, Lopez-Santiago LF, Yuan Y et al (2013) Dravet syndrome patient-derived neurons suggest a novel epilepsy mechanism. Ann Neurol 74:128–139. https://doi.org/10.1002/ana.23897
19. Mertens J, Wang Q-W, Kim Y et al (2015) Differential responses to lithium in hyperexcitable neurons from patients with bipolar disorder. Nature 527:95–99. https://doi.org/10.1038/nature15526
20. Wainger BJ, Kiskinis E, Mellin C et al (2014) Intrinsic membrane hyperexcitability of amyotrophic lateral sclerosis patient-derived motor neurons. Cell Rep 7:1–11. https://doi.org/10.1016/j.celrep.2014.03.019
21. Mertens J, Wang Q-W, Kim Y et al (2015) Differential responses to lithium in hyperexcitable neurons from patients with bipolar disorder. Nature 527:95
22. Habela CW, Song H, Ming G (2016) Modeling synaptogenesis in schizophrenia and autism using human iPSC derived neurons. Mol Cell Neurosci 73:52–62. https://doi.org/10.1016/j.mcn.2015.12.002
23. Watmuff B, Berkovitch SS, Huang JH et al (2016) Disease signatures for schizophrenia and bipolar disorder using patient-derived induced pluripotent stem cells. Mol Cell Neurosci 73:96–103. https://doi.org/10.1016/j.mcn.2016.01.003
24. Li HL, Gee P, Ishida K, Hotta A (2016) Efficient genomic correction methods in human iPS cells using CRISPR-Cas9 system. Methods 101:27–35
25. Paquet D, Kwart D, Chen A et al (2016) Efficient introduction of specific homozygous and heterozygous mutations using CRISPR/Cas9. Nature 533:125–129. https://doi.org/10.1038/nature17664

26. Avior Y, Sagi I, Benvenisty N (2016) Pluripotent stem cells in disease modelling and drug discovery. Nat Rev Mol Cell Biol 17:170–182. https://doi.org/10.1038/nrm.2015.27
27. Swinney DC, Anthony J (2011) How were new medicines discovered? Nat Rev Drug Discov 10:507–519. https://doi.org/10.1038/nrd3480
28. Zheng W, Thorne N, McKew JC (2013) Phenotypic screens as a renewed approach for drug discovery. Drug Discov Today 18:1067–1073. https://doi.org/10.1016/j.drudis.2013.07.001
29. Eder J, Sedrani R, Wiesmann C (2014) The discovery of first-in-class drugs: origins and evolution. Nat Rev Drug Discov 13:577–587. https://doi.org/10.1038/nrd4336
30. Hempel CM, Werley CA, Dempsey GT, Gerber DJ (2017) Targeting neuronal function for CNS drug discovery. Drug Discov Today Technol 23:17–25. https://doi.org/10.1016/j.ddtec.2017.03.005
31. Haggarty SJ, Silva MC, Cross A et al (2016) Advancing drug discovery for neuropsychiatric disorders using patient-speci fi c stem cell models. Mol Cell Neurosci 73:104–115. https://doi.org/10.1016/j.mcn.2016.01.011
32. Boulting GL, Kiskinis E, Croft GF et al (2011) A functionally characterized test set of human induced pluripotent stem cells. Nat Biotechnol 29:279–286. https://doi.org/10.1038/nbt.1783.A
33. Zhang Y, Pak C, Han Y et al (2013) Rapid single-step induction of functional neurons from human pluripotent stem cells. Neuron 78:785–798
34. Di Giorgio FP, Boulting GL, Bobrowicz S, Eggan KC (2008) Human embryonic stem cell-derived motor neurons are sensitive to the toxic effect of glial cells carrying an ALS-causing mutation. Cell Stem Cell 3:637–648. https://doi.org/10.1016/j.stem.2008.09.017
35. Werley CA, Brookings T, Upadhyay H et al (2017) All-optical electrophysiology for disease modeling and pharmacological characterization of neurons. Curr Protoc Pharmacol. https://doi.org/10.1002/cpph.25
36. Hochbaum DR, Zhao Y, Farhi SL et al (2014) All-optical electrophysiology in mammalian neurons using engineered microbial rhodopsins. Nat Methods 11:825–833. https://doi.org/10.1038/nmeth.3000
37. Adam Y, Kim JJ, Lou S et al (2018) All-optical electrophysiology reveals brain-state dependent changes in hippocampal subthreshold dynamics and excitability. bioRxiv. https://doi.org/10.1101/281618
38. Werley CA, Chien M-P, Cohen AE (2017) An ultrawidefield microscope for high-speed fluorescence imaging and targeted optogenetic stimulation. Biomed Opt Express 8:5794. https://doi.org/10.1364/BOE.8.005794
39. Pak CH, Danko T, Zhang Y et al (2015) Human neuropsychiatric disease modeling using conditional deletion reveals synaptic transmission defects caused by heterozygous mutations in NRXN1. Cell Stem Cell 17:316–328. https://doi.org/10.1016/j.stem.2015.07.017
40. Maroof AM, Keros S, Tyson J et al (2013) Directed differentiation and functional maturation of cortical interneurons from human embryonic stem cells. Cell Stem Cell 12:559–572. https://doi.org/10.1016/j.stem.2013.04.008
41. Ducouret P (1976) The effect of quinidine on membrane electrical activity in frog auricular fibres studied by current and voltage clamp. Br J Pharmacol 57:163–184. https://doi.org/10.1111/j.1476-5381.1976.tb07465.x
42. Alexander SPH, Striessnig J, Kelly E et al (2017) The concise guide to pharmacology 2017/18: voltage-gated ion channels. Br J Pharmacol 174:S160–S194. https://doi.org/10.1111/bph.13884
43. Roberts GKM and E (2014) Structure activity relationships of novel antiepileptic drugs. Curr Med Chem 21:722–754
44. Sandoe J, Eggan K (2013) Opportunities and challenges of pluripotent stem cell neurodegenerative disease models. Nat Neurosci 16:780–789. https://doi.org/10.1038/nn.3425